Powder electrification during pneumatic transport: the role of the particle properties and flow rates

Lise Ceresiat[a], Holger Grosshans[b], Miltiadis V. Papalexandris[a,*]

[a] *Institute of Mechanics, Materials and Civil Engineering, Université catholique de Louvain, 1348 Louvain-la-Neuve, Belgium*
[b] *Physikalisch-Technische Bundesanstalt (PTB), Bundesallee 100, 38116 Braunschweig, Germany*

Abstract

During their pneumatic transport, powders accumulate electrostatic charge due to collisions with the walls of the pipe. This phenomenon is known as triboelectric charging and may cause hazardous spark discharges. For this reason, there is a strong interest in studying various options to constrain it. However, many aspects related to this phenomenon still remain poorly understood. In this paper we report on numerical studies of the role of the particle properties and flow rates to the buildup of electric charge. The turbulent flow of the carrier gas is treated numerically via Large Eddy Simulations (LES), whereas the motion of each particle is tracked individually in the Lagrangian framework. The governing equations are endowed with four-way coupling between particles and carrier gas, as well as dynamic models for the charge exchange during wall-particle and particle-particle collisions. According to our study, an increase of the particle diameter leads to higher charge exchange during wall-particle collisions and to higher average charge per particle. Also, the Young modulus of the powder appears to be the most important material property; as it increases the powder charge drops considerably. With regard to the powder mass-loading, it has minimal impact on the average charge per particle. Finally, our simulations predicted that at sufficiently low Reynolds numbers, reducing the inlet velocity can lead to an increase of the average particle charge due to the tendency of the particles to settle at the bottom wall.

*Corresponding author.
Email address: `miltos@uclouvain.be` (Miltiadis V. Papalexandris)

Keywords: Particle-laden flows, Multiphase flows, Large Eddy Simulations, Electrostatics, Explosion safety, Triboelectric charging

1. Introduction

During their pneumatic transport, powders accumulate electrostatic charge due to collisions of the particles with the walls of the pipe. This phenomenon, known as triboelectric charging, may cause hazardous spark discharges (Glor, 2001, 2003, Shinbrot, 2014). In fact, such discharges have caused numerous dust explosions in the past with dire consequences both in terms of fatalities and property loss. On the other hand, triboelectring charging is used to our benefit in modern technological applications such as lithography and screen displays. For these reasons, there is a strong interest in studying various options to control or constrain it.

Thus far, the effect of the conveying setup on the charging process has been investigated by several authors via experiments (e.g. Smeltzer et al., 1982, Nifuku and Katoh, 2003, LaMarche et al., 2009, Fath et al., 2013, Schwindt et al., 2017) or numerical simulations (e.g. Kolniak and Kuczynski, 1989, Tanoue et al., 1999, Watano et al., 2003). These investigations helped to establish, for example, the strong influence of the transport velocity.

Several parameters in the boundary and initial conditions are also known to influence triboelectric charging. Examples include the initial particle charge (Masui and Murata, 1983, Yamamoto and Scarlett, 1986), the distribution of charge on the particle surface (Matsuyama et al., 2003), the ambient temperature (Greason, 2000), and others. Many of these parameters, however, are difficult to control in an experimental setting. As a result, many aspects underlying charge buildup are not well understood; see, for example, the discussions in the papers of Matsusaka et al. (2010) and Wei and Gu (2015). This applies especially to conveying of dense mixture where the solid accumulates a high amount of charge. In this type of flows, as Fotovat et al. (2017) and Klinzing (2018) elaborated in their recent reviews, the emerging electric has a strong influence on both the charge transfer and the emerging particle flow pattern.

It is also generally admitted that the mechanical and electrical properties of the powder and pipe materials also play a significant role to the charging process, although relatively few works have examined in detail this issue. For example, Harper (1951) examined the influence of the type of material on the contact potential difference due to different work functions. His investigations involved a chromium sphere in contact with a sphere made of another metal. Subsequently, Davies (1969) and Murata and Kittaka (1979) studied the charge exchange during the contact between a metallic and an insulator surface. Later on, various authors explored the effect of the materials involved in the charge exchange between two insulator surfaces; see, for example, Lowell and Rose-Innes (1980), Lee (1994), Bailey (2001) and Mehrani et al. (2007). On the basis of these developments, researchers have examined various strategies of controlling powder electrification. For example Matsusaka et al. (2007, 2008) considered combining pipes of two materials or employing a pipe made of two materials. Another option that has been put forward is the addition of anti-static powders; see, for example Wang et al. (2000) as well as Zhu et al. (2003, 2004). Despite these efforts, a lot of questions related to the role of the material properties currently remain open.

In a recent study, Grosshans and Papalexandris (2016a) studied numerically various factors influencing the charging process via Large Eddy Simulations (LES). In this work, the results of the simulations were analyzed with the Design of Experiments methodology and confirmed the role of the transport velocity and pipe diameter. The effect of the pipe diameter was also studied in the recent experiments of Schwindt et al. (2017). In another relevant study, Grosshans and Papalexandris (2017b) performed LES of powder electrification and examined the role of the electrical properties of the particles.

The focus of the present study, however, is different. Herein we examine the role of the mechanical properties of the powder to triboelectric charging. More specifically, we analyze the influence of the particle diameter, Young modulus, density and mass-loading of the powder. We also explore further and provide new physical insight on the mechanisms underlying the dependence of the powder charge on the inlet velocity. Our study is based on Large Eddy Simulations combined with parametric studies with respect to the properties of interest. To the best of our knowledge, such parametric studies are currently unavailable in the literature.

The paper is organized as follows. The mathematical model and its validation are presented in Section 2. The numerical setup is given in Section 3. The numerical results are presented and analysed in Section 4. Finally, Section 5 concludes.

2. Mathematical model and validation

The mathematical model used in the study has been described in detail by Grosshans and Papalexandris (2016a,b) and is summarized below. The flow of the carrier gar (air) is described by the constant-density Navier-Stokes equations with an additional term to account for momentum exchange between the air and the particles in the form of aerodynamic drag. According to our approach, these equations are solved numerically in the Eulerian framework. On the other hand, the transport of the powder is modeled via the Discrete Element Method (DEM), according to which the motion of each particle is tracked individually in the Langrangian framework. Momentum exchange between the two phases and between particles during collisions is taken into account via a four-way coupling. The suitability of this approach to treat pneumatic conveying processes has been demonstrated and discussed in detail by Zhu et al. (2008) and Zhou et al. (2010).

According to the methodology of LES, the constant-density Navier-Stokes equations are filtered in space. Thus, the large turbulent scales of the flow (which also carry most of the turbulent kinetic energy) are directly resolved by the computational grid, whereas the smaller ones are suitably modelled. The filtered equations read

$$\nabla \cdot \boldsymbol{u} = 0\,, \tag{1}$$

$$\frac{\partial \boldsymbol{u}}{\partial t} + (\boldsymbol{u} \cdot \nabla)\boldsymbol{u} = -\frac{1}{\rho}\nabla p + (\nu + \nu_t)\,\nabla^2 \boldsymbol{u} + \boldsymbol{F}_\mathrm{s}\,. \tag{2}$$

In the above system, $\boldsymbol{u}$ is the spatially-filtered velocity vector, ρ is the density and ν is the viscosity coefficient of the gas. The source term $\boldsymbol{F}_\mathrm{s}$ accounts for the aerodynamic drag. More specifically, its integral over a control volume is equal to the opposite of the sum of the aerodynamic drag forces that act on the particles that are located inside the control volume.

Further, ν_t is the eddy viscosity and represents the transport and dissipation of kinetic energy to the subgrid (unresolved) turbulent structures. It is calculated via the dynamic approach of Germano et al. (1991), combined the least-square technique and averaging in the streamwise direction as proposed by Lilly (1992). In order to reduce the requirements on the grid in the near-wall region, we employ the wall model of Grötzbach (1987).

The momentum Eq. (2) is integrated in time via an implicit second-order backward scheme. With regard to spatial discretization, the convective terms are approximated via a Weighted Essentially Non Oscillatory (WENO) upwind scheme that is up to fifth-order accurate (Jang and Shu, 1996), whereas the diffusive terms are approximated via fourth-order central differences. The pressure field is evaluated via a projection method. This amounts to taking the divergence of Eq. (2), introducing the zero-divergence condition (1) to it, and finally solving numerically the resulting Poisson equation for the pressure. The reader is referred to Gullbrand et al. (2001) for further details concerning the numerical implementation of the flow solver.

As regards the particulate phase, we assume that it consists of spherical, monodisperse particles that are made of the same material. For numerical purposes, each particle is represented as a material point in space. The acceleration of a particle is calculated by the following balance of forces,

$$\frac{d\boldsymbol{u}_{\mathrm{p}}}{dt} \;=\; \boldsymbol{f}_{\mathrm{aero}} + \boldsymbol{f}_{\mathrm{g}} + \boldsymbol{f}_{\mathrm{coll}} + \boldsymbol{f}_{\mathrm{el}}\,. \tag{3}$$

In this expression, the terms $\boldsymbol{f}_{\mathrm{aero}}$, $\boldsymbol{f}_{\mathrm{g}}$, $\boldsymbol{f}_{\mathrm{coll}}$, and $\boldsymbol{f}_{\mathrm{el}}$ represent the acceleration due to aerodynamic drag, gravity, collisional force and the electric-field force, respectively. The aerodynamic force acting on one particle is computed via the relation

$$\boldsymbol{f}_{\mathrm{aero}} \;=\; -\frac{3\rho_{\mathrm{air}}}{4\rho_{\mathrm{p}} d_{\mathrm{p}}} c_{\mathrm{D}} |\boldsymbol{u}_{\mathrm{rel}}| \boldsymbol{u}_{\mathrm{rel}}\,, \tag{4}$$

where ρ_{air} and ρ_{p} are the densities of the air and particle, respectively, and $\boldsymbol{u}_{\mathrm{rel}}$ is the relative velocity of the particle with respect to the surrounding air, $\boldsymbol{u}_{\mathrm{rel}} = \boldsymbol{u} - \boldsymbol{u}_{\mathrm{p}}$. For the computation of the drag coefficient c_{D} we employ the well-known correlation of Schiller and Naumann (1935). We note that $\boldsymbol{u}_{\mathrm{rel}}$ is defined on the basis of the spatially-filtered velocity $\boldsymbol{u}$ and that the above expression for $\boldsymbol{f}_{\mathrm{aero}}$ does not include a subgrid-scale model for the term $|\boldsymbol{u}_{\mathrm{rel}}|\boldsymbol{u}_{\mathrm{rel}}$.

The collisional force takes into account both particle-particle and wall-particle collisions. Particle-particle collisions are assumed to be fully elastic. On the other hand, the reflections of particles off the pipe walls are assumed to be imperfectly elastic. Accordingly, the component of the particle velocity normal to the wall changes sign and, due to restitution, reduces to

$$u'_{\mathrm{p,n}} \;=\; -k_{\mathrm{e}} u_{\mathrm{p,n}}\,, \tag{5}$$

where $u'_{\mathrm{p,n}}$ is the particle normal velocity component after impact and k_{e} is the restitution ratio of the particle (Lackmann, 2007).

Due to the finite size of the domain under investigation herein, the number of wall-particle collisions and, therefore, the expected charge per particle is rather low. As shown by (Kolehmainen et al., 2018), this fact allows to neglect polarization effect. Therefore, the acceleration $\boldsymbol{f}_{\mathrm{el}}$ of one particle is due to the Coulomb force caused by the electric field $\boldsymbol{E}$ that is generated by the ensemble of the charged particles. It is given by

$$\boldsymbol{f}_{\mathrm{el}} = \frac{Q}{m_{\mathrm{p}}} \boldsymbol{E} , \tag{6}$$

where Q and m_{p} are the charge and the mass of the particle, respectively. The electric-field strength $\boldsymbol{E}$ is written in terms of the gradient of the electric potential ϕ: $\boldsymbol{E} = -\nabla\phi$. Thus, Gauss's law yields the following Poisson equation for ϕ,

$$\nabla^2 \phi = \frac{\rho_{\mathrm{el}}}{\epsilon_0} , \tag{7}$$

where ϵ_0 is the permittivity of the carrier gas and ρ_{el} the volumetric electric charge density. The latter quantity is computed by summing the charges of all particles inside a control volume (e.g. a computational cell),

$$\int_{V_{\mathrm{cv}}} \rho_{\mathrm{el}} \, dV_{\mathrm{cv}} = \sum_{i=1}^{N} Q_i , \tag{8}$$

with N being the number of particles inside the control volume at a given time.

During pneumatic transport of powders, different types of charge exchange may occur. The first one is via particle-particle collisions, and it requires that the colliding particles carry different pre-charges. The second one is via collisions of the particles with the walls of the pipe. Their calculation is based on the analogy of charging/decharging of a capacitor, as proposed by Soo (1971).

Since the particles are made of the same material they have identical resistivities and their surfaces have identical work functions. Let us denote by "1" and "2" two particles that are in course of collision and by Δt_{pp} the contact time during collision. Then, the charge exchanges for these particles, denoted by ΔQ_1 and ΔQ_2 respectively, are given by

$$\Delta Q_1 = \frac{C_1 C_2}{C_1 + C_2} \left(\frac{Q_2}{C_2} - \frac{Q_1}{C_1} \right) \left(1 - \mathrm{e}^{-\Delta t_{\mathrm{pp}}/\tau_{\mathrm{pp}}} \right) = -\Delta Q_2 . \tag{9}$$

With regard to the above relation, the electric capacity C_1 of the spherical particle "1" is given by (Soo, 1971)

$$C_1 = 4\pi\varepsilon_0 r_{\mathrm{p},1}\,, \tag{10}$$

with $r_{\mathrm{p},1}$ being the radius of the particle "1". An analogous expression holds for the electric capacity C_2 of the spherical particle "2". In our case, since all particles have the same radius, then their electric capacities are equal.

The charge relaxation time τ_{pp} that appears in Eq. (9) is calculated from the following expression,

$$\tau_{\mathrm{pp}} = \frac{C_1 C_2}{C_1 + C_2}\frac{r_{\mathrm{p},1} + r_{\mathrm{p},2}}{A_{12}}\,\varphi_{\mathrm{p}}\,, \tag{11}$$

where φ_{p} denotes the resistivity of the particles. The calculation of the contact surface A_{12} is based on the elastic theory of Hertz according to which

$$A_{12} = \frac{\pi\, r_{\mathrm{p},1} r_{\mathrm{p},2}}{r_{\mathrm{p},1} + r_{\mathrm{p},2}}\,\alpha_{12}\,, \tag{12}$$

with

$$\alpha_{12} = r_{\mathrm{p},1} r_{\mathrm{p},2}\left(\frac{5}{8}\pi\rho_{\mathrm{p}}(1 + k_{\mathrm{e}})|\boldsymbol{u}_{\mathrm{p},12}|^2 \frac{\sqrt{r_{\mathrm{p},1} + r_{\mathrm{p},2}}}{r_{\mathrm{p},1}^3 + r_{\mathrm{p},2}^3}\frac{1 - \nu_{\mathrm{p}}^2}{E_{\mathrm{p}}}\right)^{2/5}\,. \tag{13}$$

In the above relation, $\boldsymbol{u}_{\mathrm{p},12}$ is the relative velocity of the two particles. Also, k_{e}, ν_{p} and E_{p} stand for the restitution ratio, the Poisson ratio and the Young modulus of the particles, respectively.

Lastly, the calculation of the contact time Δt_{pp} that appears in Eq. (9) is also based on the theory of Hertz, according to which

$$\Delta t_{\mathrm{pp}} = \frac{2.94}{|\boldsymbol{u}_{\mathrm{p},12}|}\,\alpha_{12}\,. \tag{14}$$

As regards charge exchange during wall-particle collisions, its computation is based on the model of John et al. (1980) which stipulates that the total exchange ΔQ_{pw} consists of the dynamic charge transfer ΔQ_{c} and the contribution due to the particle pre-charge, ΔQ_{t},

$$\Delta Q_{\mathrm{pw}} = \Delta Q_{\mathrm{c}} + \Delta Q_{\mathrm{t}}\,. \tag{15}$$

Herein we assume that the radius of the particles is much larger than the contact area during impact. Therefore, the dynamic charge transfer Δt_{pw} is modeled in a manner analogous to the charging of a parallel-plate capacitor,

$$\Delta Q_{\mathrm{c}} \;=\; C\,V_{\mathrm{c}}\left(1 - e^{-\Delta t_{\mathrm{pw}}/\tau_{\mathrm{pw}}}\right)\,, \tag{16}$$

where C, V_{c}, τ_{w} and Δt_{pw} are the electrical capacity, wall-particle contact potential, charge-relaxation time and wall-particle contact time, respectively. According to the model of a parallel-plate capacitor that we adopted in the present study, C is given by

$$C \;=\; \frac{\varepsilon_0 A_{\mathrm{pw}}}{h}\,, \tag{17}$$

where A_{pw} is the plate surface area and h is the distance between the two plates. The plate surface corresponds to the contact area between the particle and the wall. On the basis of the elastic theory of Hertz, it is given by

$$A_{\mathrm{pw}} \;=\; \pi r_{\mathrm{p}} \alpha_{\mathrm{pw}}\,, \tag{18}$$

with

$$\alpha_{\mathrm{pw}} \;=\; r_{\mathrm{p}} \left(\frac{5}{8}\pi\rho_{\mathrm{p}}(1+k_{\mathrm{e}})|\boldsymbol{u}_{\mathrm{p}}|^2 \left(\frac{1-\nu_{\mathrm{p}}^2}{E_{\mathrm{p}}} + \frac{1-\nu_{\mathrm{w}}^2}{E_{\mathrm{w}}} \right) \right)^{2/5}\,, \tag{19}$$

where ν_{w} and E_{w} are the Poisson ratio and Young modulus of the wall, respectively. Also, following the arguments of John et al. (1980) and Kolniak and Kuczynski (1989), the distance h between the capacitor's plates is chosen to be 10^{-9} m. This is assumed to be of the order of the range of repulsive molecular forces due to surface irregularities.

The contact time Δt_{pw} in Eq. (16) is also calculated by the theory of Hertz as follows,

$$\Delta t_{\mathrm{pw}} = \frac{2.94}{|\boldsymbol{u}_{\mathrm{p}}|}\,\alpha_{\mathrm{pw}}\,. \tag{20}$$

For the charge relaxation time in Eq. (16) we employ the relation provided by John et al. (1980),

$$\tau_{\mathrm{pw}} = \varepsilon\,\varepsilon_0\,\varphi_{\mathrm{p}} \tag{21}$$

where ε is the relative permittivity of the system and φ_{p} is the resistivity of the particle; see also the relevant discussion in Grosshans and Papalexandris (2017b).

With regard to the contact potential V_c, it is well known that it exhibits spatial and temporal variations; see, for example Baytekin et al. (2011). These are due to a number of factors such as surface roughness of particles and walls, inhomogeneities in the chemical composition, and others. Nonetheless, currently there is no clear consensus on the influence of these factors to the contact potential or how to take them into account. Accordingly, we assume herein that V_c is constant and equal to 1 V; see also Kolniak and Kuczynski (1989).

Finally, the charge of a given particle is assumed to be uniformly distributed on its surface, so that the pre-charge transfer across the the contact area reads

$$\Delta Q_\mathrm{t} = \frac{1}{4}\frac{\alpha_\mathrm{pw}}{r_\mathrm{p}}\, Q\,, \tag{22}$$

with α_pw given by Eq. (19). More elaborate models that do not assume uniform contact have also been developed recently; see, for example, Lacks and Duff (2008), Grosshans and Papalexandris (2016c) and references therein. Nonetheless, the assumption of uniform charge distribution on the particle surface is deemed satisfactory for the purposes of our study.

At this point, a few comments about the interaction between the electric and flow fields in the problem of interest are appropriate. We first remark that the carrier gas (air) is considered to be electrically neutral. For this reason, the flow turbulence is not affected by the electric field that is generated by the charged particles. Moreover, since the mixtures considered herein are very dilute, the flow turbulence is only slightly influenced by the motion of the particles, as experessed by the aerodynamic-drag term $\boldsymbol{F}_\mathrm{s}$ in Eq. (2).

Finally, it must be mentioned that in our study we have assumed that initially the particles carry no charge. For this reason, the pre-charge transfer ΔQ_t during wall-particle collisions is small, cf. (22). In practice, this implies that the pre-charge transfer is always smaller than the dynamic charge transfer and, therefore, the electrostatic charge will not reach the equilibrium state. Indeed, according to our estimations, each particle should collide several hundred times with the wall before its charge gets saturated. This, however, does not occur because, as evidenced by our simulations, the particles collide only a few times with the wall before exiting the pipe.

The Eulerian-Lagrangian flow solver (excluding electrostatic effects) employed in the present study has been previously tested by Grosshans and Papalexandris (2016b) against the experimental data Tsuji et al. (1984) for pneumatic transport of polystyrene particles. The numerical grid-refinement studies reported therein showed that simulations with sufficiently fine grids yield accurate predictions as regards both the average and the fluctuating velocity components. In those simulations the solid-to-gas volume ratio per cell was maintained sufficiently low so that the powder could be modeled by the Discrete Element Method (Sirignano, 1999, Grosshans et al., 2014).

The electrostatics solver is based on a particle-mesh method for the computation of the electric field and the forces between particles. Another choice would be to employ the P3M method (Hockney and Eastwood, 1989) since, according to a recent study (Yao and Capecelatro, 2018), it gives more accurate results for turbulent flows with charged particles. In fact, in the context of our numerical studies, we examined various approaches to compute the forces on the particles and we previously developed a scheme similar to P3M (Grosshans and Papalexandris, 2017c). However, in the problem under study, any given particle experiences only a limited number of wall collisions, thus it accumulates only a small amount of charge. Moreover, the mixtures examined herein are quite dilute. Due to these reasons, the forces between particles are small. As a result, the improvement offered by P3M-based methods was modest and could not justify the additional computational cost.

With regard to validation of the electrostatics model, we have performed comparisons with the experiments of Matsuyama and Yamamoto (1995) on the charge exchange between single PTFE particles and a brass plate. These comparisons are detailed in Grosshans and Papalexandris (2016c) and are summarized herein. In the experiments of Matsuyama and Yamamoto (1995), the particle diameter was 3.2 mm, the impact velocity was 11.4 m/sec and each particle carried a different amount of initial charge. Our numerical results for the charge exchange during impact are plotted in Figure 1 along with the experimental data. From this figure we can see that our model predicts well the resulting impact charge. In particular, the data points follow the linear charge relation postulated by Masui and Murata (1983) and Yamamoto and Scarlett (1986). In this figure we also observe that the experiments exhibit a scatter around the charging line. This can be explained either by fluctuating impact conditions or, more likely, by a non-uniform pre-charge.

Furthermore, in an earlier study (Grosshans and Papalexandris, 2016a), we performed simulations of powder electrification in a pipe with the aforementioned models and algorithms and compared our predictions for the average charge per particle with the experimental data of Watano et al. (2003). The comparisons suggested that the dependency of the charge on the con-

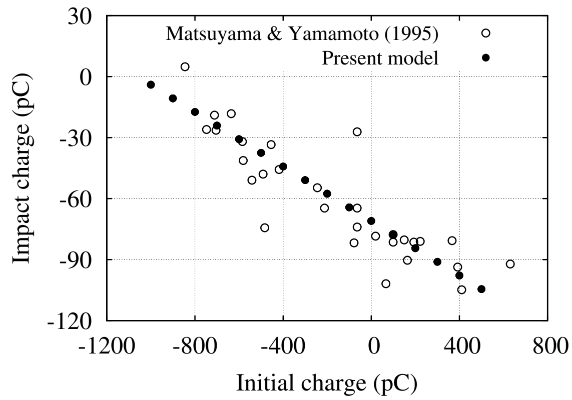

Figure 1: Results of the single particle charging experiment by Matsuyama and Yamamoto (1995) and the electrostatics model. The figure shows that the model predicts well the dependence of the impact charge on the initial particle charge. Note that for a better visualization not all data points are shown. (Modified from Grosshans and Papalexandris (2016c); © 2016, Elsevier)

veying air velocity is accurately computed. However, the measured absolute powder charge was higher than the calculated one, which was attributed to a non-zero initial particle charge in the experiments. The combined fluid flow-electrostatics solver has been successfully used to simulate triboelectric charging both in wall-bounded flows over a wide range of Reynolds numbers (Grosshans and Papalexandris, 2017a) and in external flows, including charge accumulation in helicopters hovering in dusty atmospheres (Grosshans et al., 2017, 2018).

3. Numerical set-up and material parameters

The present work focuses on the effect of certain particle properties and flow rates on powder electrification during pneumatic transport. More specifically, we have conducted parametric studies with respect to the particle diameter d_p and the fundamental mechanical properties of the powder's material, namely, the Poisson ratio ν_p, the Young modulus E_p and the density ρ_p. Also, in terms of flow rates, we have considered the effects of the powder mass-loading and the inlet velocity. In our simulations, the dimensions of the pipe, the properties of the carrier gas and the electric properties of the

Parameter	Value
Pipe length	$L = 1$ m
Pipe diameter	$D = 40$ mm
Particle restitution ratio	$k_{\mathrm{e}} = 0.95$
Density of air	$\rho_{\mathrm{p}} = 1.1$ kg m^{-3}
Kinematic viscosity of air	$\nu = 1.46\times10^{-5}$ m^{2}s^{-1}
Vacuum permittivity	$\epsilon_0 = 8.854\times10^{-12}$ F m^{-1}
Effective separation	$h = 10^{-9}$ m
Contact potential	$V_{\mathrm{c}} = 1$ V
Relative permittivity	$\epsilon = 5$
Particle resistivity	$\varphi_{\mathrm{p}} = 8{\cdot}10^8$ Ωm

Table 1: Numerical values of the parameters that have been kept constant in the present study.

powder have been kept constant. Their numerical values are listed in Table 1. Also, the pipe wall is assumed to be perfectly grounded.

In our study, we have performed a total of 11 different cases by letting vary the afore-mentioned parameters of interest. The numerical values of these parameters are provided in Table 2 for all cases considered herein. Case 1 is the *reference* case of our study and corresponds to the pneumatic transport of PMMA powder through a steel pipe with a powder flow rate equal to 10 g/s and a bulk velocity equal to 30 m/s.

In the first 8 cases the powder mass-loading has been kept constant. Accordingly, the number of injected particles N is given by the following relation

$$\dot{m} = \frac{N m_{\mathrm{p}}}{\tau}, \tag{23}$$

where m_{p} is the mass of one particle and τ stands for the duration of the simulation. In our simulations, we set τ=1 s. On the other hand, for the last 3 cases the number of injected particles has been kept constant but we let the inlet velocity vary.

In our simulations we employ a uniform Cartesian grid consisting of 200 points in the streamwise direction and 30×30 points on the plane normal to the flow direction. The distance of the first cell from the the wall is larger than one wall-unit, which necessitates the introduction of wall model. As mentioned above, the near-wall structures are accounted for by the wall model of Grötzbach (1987), assuming that the mean velocity profile verifies

Case #	d_{p} [µm]	E_{p} [MPa]	ρ_{p} [kg/m^3]	ν_{p}	$\dot{m}$ [g/s]	u_{in} [m/s]
1	300	3000	1090	0.4	10	30
2	150	3000	1090	0.4	10	30
3	600	3000	1090	0.4	10	30
4	1200	3000	1090	0.4	10	30
5	300	1300	900	0.41	10	30
6	300	2400	1200	0.39	10	30
7	300	3000	1090	0.4	5	30
8	300	3000	1090	0.4	50	30
9	300	3000	1090	0.4	3.33	10
10	300	3000	1090	0.4	6.7	20
11	300	3000	1090	0.4	13	40

Table 2: Numerical values of the varying parameters for each case of the present study.

the logarithmic law. It is worth noting that this model does not account for turbulence modulation by the particles at the subgrid scale.

In all cases the Courant number is set equal to 0.25. The initial condition consists of the average turbulent velocity profile that corresponds to the given inlet velocity upon which we superimposed small random perturbations. The particles of the powder are injected at the inlet and at random directions. The initial velocity of a given particle is set equal to the gas velocity at the particle location.

4. Results and discussion

4.1. Effect of the particle diameter

The particles of the powder become electrically charged because they collide with the wall of the pipe that is made from a different material. Due to the different work function of the surfaces of the two materials (e.g. PMMA and steel), a gradient in the electrostatic potential emerges upon impact. In turn, this leads to the transfer of electrons, hence electric charge, from the wall to the particles. Subsequently, charge is transported away from the walls either via particle-bound charge transport or via inter-particle charge diffusion (Grosshans and Papalexandris, 2017a, 2018).

For the problem in hand, the charge carriers are electrons. We also assume that due to the different Fermi levels of the materials involved, the net transfer of electrons is from the wall to the particles. Accordingly, the charge accumulated by the particles is of negative sign. On the other hand, according to the convention adopted herein, the electron transfer from the wall to the particles is of positive sign because it represents flux of electrons toward the two-phase system.

For Case 1 (reference case), in Fig. 2 we show snapshots of the electrical charge of the particles at the outlet of the pipe ($x = 1$m) and at two different time instances, namely, t=0.03 s and t =1 s. In this figure it can be observed that most of the particles that carry significant charges are located in the near-wall region. This is attributed, at least partially, to the phenomenon of turbophoresis according to which the particles tend to segregate in regions of reduced turbulence levels (Caporaloni et al., 1975, Reeks, 1983). In other words, upon impact with the pipe-walls, the charged particles remain concentrated in the near-wall region; see also the relevant discussion in (Grosshans and Papalexandris, 2017a). The instantaneous streamwise (axial) velocity component of the particles along the pipe at the same instances are depicted in Fig. 3. From this figure we can confirm that due to aerodynamic drag that tends to equilibrate the velocities of the two phases, the velocity distribution of the particles is very similar to the one of the carrier gas.

In Fig. 4 we provide plots of the probability density functions (pdf) of the charge per particle exiting the pipe for the four different values of d_p considered in our study (Cases 1-4). We can readily observe the large increase of charge with the particle diameter. In fact, according to our simulations, when d_p is doubled, the particle electrification increases tenfold. This is to be expected because the contact surface during wall-particle collisions, A_pw, scales with the square of the particle diameter; see Eqs. (18) and (19). Moreover, and according to Eqs. (19) and (20), the contact time Δt_pw scales linearly with the particle diameter. Because of these two factors, the dynamic charge transfer ΔQ_c, given in Eq. (16), increases rapidly with d_p. The values of the electric charge per exiting particle, as well as the number of injected and exiting particles during the simulation are provided in Table 3. These data confirm the large dependence of powder electrification with the particle diameter.

From Fig. 4 we can also see that each pdf consists of two distinct regions: the one at the right corresponds to particles containing zero or very small charges, while the region at the left corresponds to particles carrying noticeable charge. This may be attributed to the fact that, as elaborated above, there are two distinct charge-exchange mechanisms. More specifically,

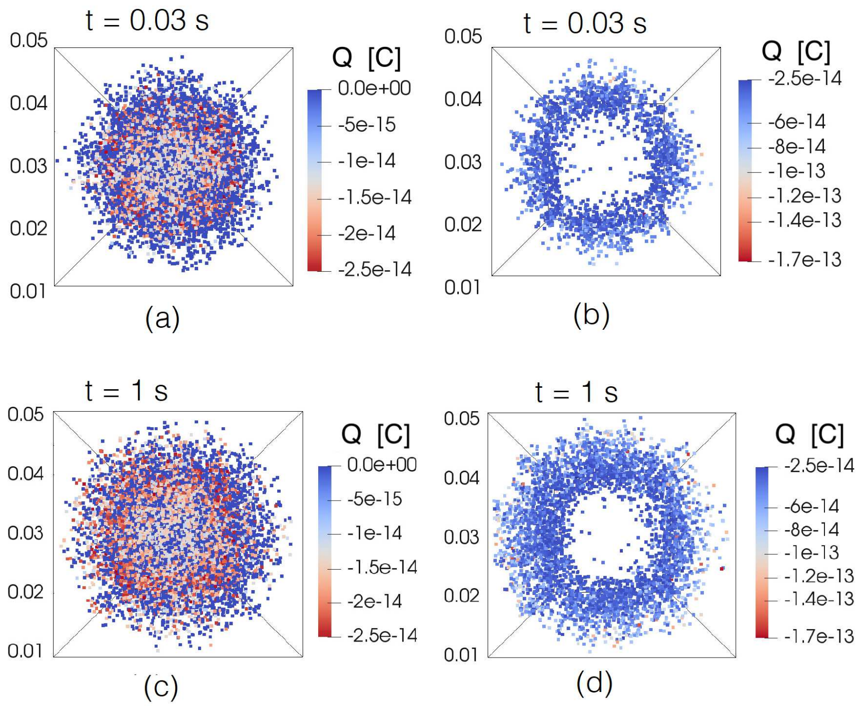

Figure 2: Case 1. Snapshots of the charge carried by the particles at the pipe outlet for the reference case, i.e. pneumatic transport of PMMA powder in a steel pipe. (a) and (b) t=0.03 s; (c) and (d) t =1 s. For visualisation purposes, subfigures (a) and (c) show the lightly charged particles, whereas subfigures (b) and (d) show the significantly charged ones.

the powder accumulates charge during wall-particle collisions, but particle-particle collisions redistribute the charge over the entire powder. This means that in the course of time these collisions will lead to smaller charge exchange. We therefore conclude that the right region in the pdfs corresponds to particles that accumulated their charge mostly via particle-particle collisions.

Moreover, from Fig. 4 we can attest that the percentage of particles that belong to the right region of the pdfs decreases as d_{p} increases. This is corroborated by the data provided in Table 3 according to which the amplitude of the charge per exiting particle Q^{av} increases with d_{p}. This phenomenon can be explained by the fact that under constant powder mass-loading, the number of particles increases as the d_{p} becomes smaller. In turn, more par-

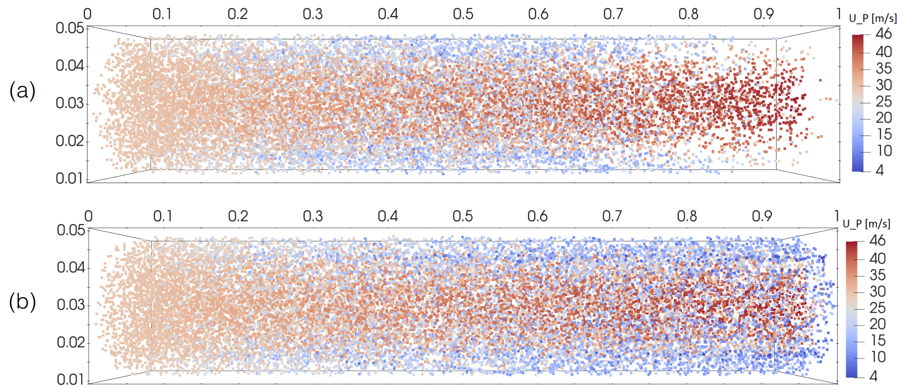

Figure 3: Case 1. Snapshots of the axial velocities of the PMMA particles along the steel pipe. (a) t=0.03 s; (b) t =1 s. For better visualization purposes, the radial coordinate has been magnified by a factor of five.

Case	N_{in}	N_{out}	$\Delta Q_{\mathrm{pw}}^{\mathrm{av}}$ [pC]	$\lvert Q^{\mathrm{av}}\rvert$ [pC]	$\lvert Q^{\mathrm{t}}\rvert$ [μC]	$\lvert Q_{\mathrm{n}}^{\mathrm{t}}\rvert$ $[\frac{\mu\mathrm{C}}{\mathrm{m}^2}]$
2	5471421	4316713	0.0046	0.0039	0.0168	0.0554
1	684168	508450	0.0243	0.0204	0.0104	0.0723
3	85518	59186	0.1694	0.1917	0.0113	0.1695
4	10691	6875	1.2232	1.7964	0.0124	0.3971

Table 3: Effect of the particle diameter on powder electrification. N_{in} and N_{out} are the numbers of injected and exiting particles during the simulation. $\Delta Q_{\mathrm{pw}}^{\mathrm{av}}$ is the average charge transfer per wall-particle collision, Q^{av} is the average charge per exiting particle, Q^{t} is the total charge of the exiting particles, and $Q_{\mathrm{n}}^{\mathrm{t}}$ is the total charge of the exiting particles normalized by the powder's surface area.

ticles imply more particle-particle collisions and, therefore, a more uniform distribution of electric charge among particles. Consequently, as d_{p} decreases, there is a much higher percentage of particles that carry small amounts of charge.

It is also interesting to observe that for Cases 3 and 4 the charge per exiting particle is higher than the charge exchange per wall-particle collision. This implies that, for these cases, there is a large number of particles that collided multiple times with the wall, thereby increasing the overall charge of the powder.

Further, and according to the data provided in Table 3, the total charge Q^{t} of the exiting particles is maximized for the smallest diameter, i.e. in

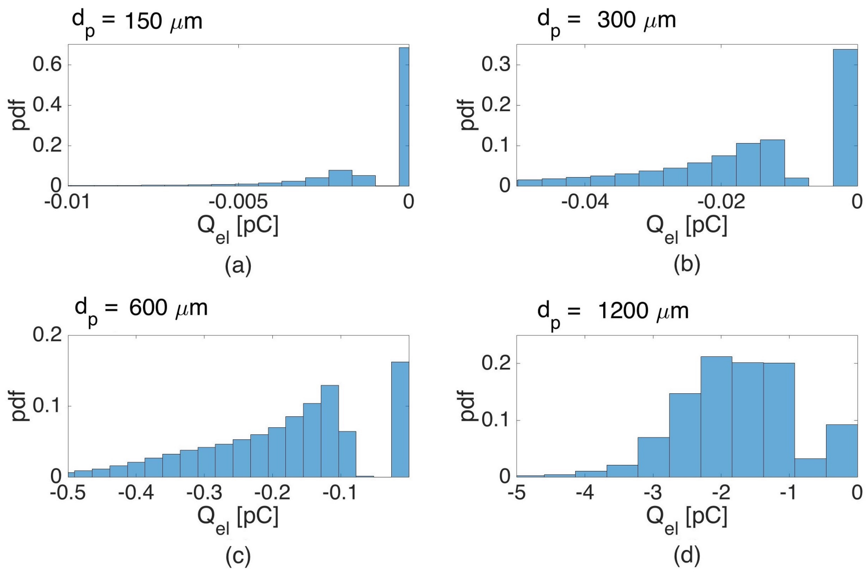

Figure 4: Effect of the particle diameter on powder electrification. Probability density function (pdf) of the charge per exiting particle $Q_{\rm el}$ at the outlet of the pipe for different particle diameters. (a) Case 2, $d_{\rm p} = 150$ μm; (b) Case 1, $d_{\rm p} = 300$ μm; (c) Case 3, $d_{\rm p} = 600$ μm; (d) Case 4, $d_{\rm p} = 1200$ μm.

Case 2 with $d_{\rm p} = 150$ μm. In other words, the most efficient accumulation of charge occurs when the powder consists of many small particles. In this case, the charge is more or less uniformly distributed among particles, with each particle carrying a small amount of charge. Nonetheless, $Q^{\rm t}$ does not decrease monotonically with $d_{\rm p}$. In fact, our parametric study shows that $Q^{\rm t}$ is minimized for $d_{\rm p} = 300$ μm but then it increases slowly at higher particle diameters. This is due to the two opposite consequences of increasing the particle diameter: on the one hand we have fewer particles and thus fewer wall-particle collisions, but on the other hand the particles are larger and thus wall-particle collisions lead to higher charge exchange. The last observation can be directly confirmed from Fig. 5 which shows plots of the pdf of the charge exchange during a wall-particle collision for Cases 1-4.

As regards comparisons with available data, Saleh et al. (2011) performed experiments on the electrification of glass particles in polymer pipes (teflon and nylon) and studied the effect of several parameters, including the particle diameter. Those authors considered the charge transfer between walls and uncharged particles (i.e. the first impact of particles with the walls) normalized by the powder surface, $Q^0_{\mathrm{pw,n}}$. On the basis of their measurements, they proposed a correlation between $Q^0_{\mathrm{pw,n}}$ and d_{p} in the form of a power law whose exponent is equal to 1.5. In Fig. 6 we have plotted our numerical results of $Q_{\mathrm{pw,n}}$ for the various d_{p} and their least-square interpolation. The interpolation reads $Q^0_{\mathrm{pw,n}} = a\left(\frac{d_{\mathrm{p}}}{2}\right)^n$ where $a = 920.07$, $n = 1.13$. In this relation, $Q^0_{\mathrm{pw,n}}$ is measured in μC and d_{p} is measured in m. The exponent of this interpolation is satisfactorily close to the one of the correlation proposed by Saleh et al. (2011).

4.2. Effect of the material properties

The effect of the material properties of the powder to its electrification is assessed via simulations of Cases 5 and 6. In these Cases, we modified the values of the material density, Young modulus and Poisson ratio have been modified with respect to the ones of Case 1 for PMMA powder. The values for Case 5 are close to the ones for Polypropylene, whereas the values of Case 6 are close to the ones for Polycarbonate. It should be noted that since we

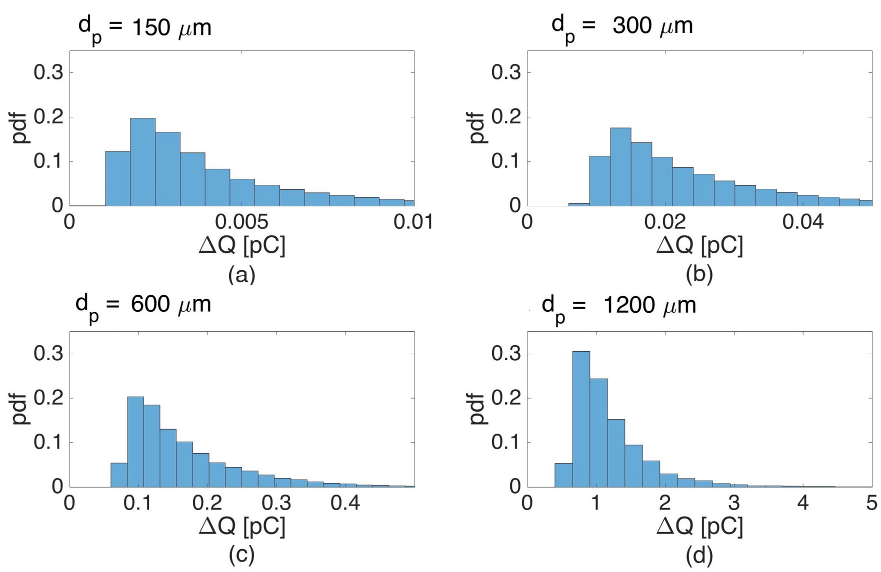

Figure 5: Effect of the particle diameter on powder electrification. Probability density function (pdf) of the charge exchange ΔQ during wall-particle collisions. (a) Case 2, d_{p} = 150 μm; (b) Case 1, d_{p} = 300 μm; (c) Case 3, d_{p} = 600 μm; (d) Case 4, d_{p} = 1200 μm.

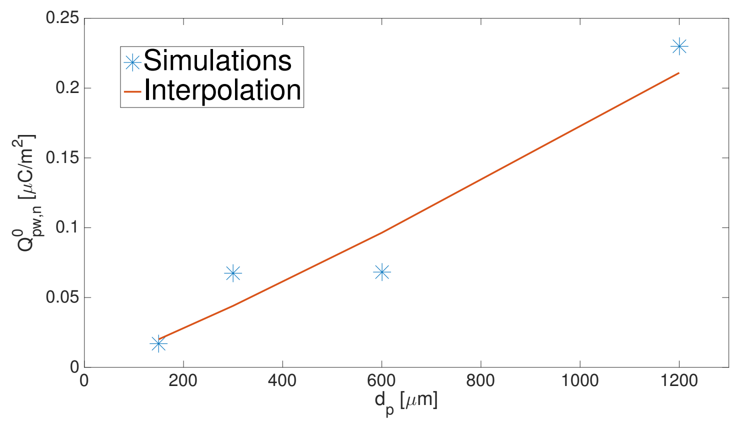

Figure 6: Effect of the particle diameter on powder electrification. Numerical results and least-squares interpolation of the charge transfer between walls and uncharged particles, normalized by the powder surface $Q^0_{\rm pw,n}$.

have kept the mass flow-rates constant, then the number of injected particles varies linearly with the density of the material; see Table 4. For this reason, our analysis is based on the charge accumulated per particle.

Upon examination of the electrostatics model, it can be deduced that the most sensitive parameters with respect to the material properties are α_{12} and $\alpha_{\rm pw}$ which are defined in Eqs. (13) and (19), respectively. Both of these parameters increase when the Young modulus $E_{\rm p}$ decreases. This implies that, according to Eqs. (14) and (20), the contact times of collisions $\Delta t_{\rm pp}$ and $\Delta t_{\rm pw}$ become longer as $E_{\rm p}$ decreases. Consequently, the charge exchanges during both particle-particle and wall-particle collisions increase as $E_{\rm p}$ decreases.

Moreover, when $E_{\rm p}$ becomes smaller, the material can undergo larger deformations. Consequently, the contact surfaces in both wall-particle and particle-particle collisions get larger, thereby leading to higher powder electrification and higher charge exchanges. This can be directly confirmed from the numerical results listed in Table 4 for the average charge per exiting particle transferred from the wall $\Delta Q^{\rm av}_{\rm pw}$, the amplitude of the average charge per particle $|Q^{\rm av}|$, and the total charge normalized by the powder's surface area $Q^{\rm t}_{\rm n}$. All these three quantities increase monotonically as the Young modulus $E_{\rm p}$ decreases.

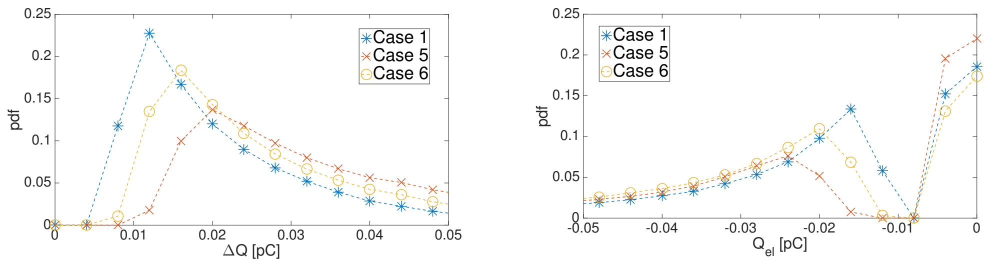

(a) (b)

Figure 7: Effect of the material properties on powder electrification. (a) Probability density function (pdf) of the charge exchange ΔQ during wall-particle collisions. (b) Probability density function (pdf) of the electric charge Q_{el} per exiting particle.

The above conclusion is corroborated by the plots in Fig. 7(a). In this figure we have plotted the computed pdf of the charge exchange during wall-particle collisions for Cases 1, 5, and 6. According to these plots, the probability that these collisions lead to significant charge exchange is the highest for Case 5 which corresponds to the smallest E_{p}. It is worth mentioning that simulations of tribolectric charging in fluidized beds also predicted that lower values of E_{p} increase the charge transfer during particle-particle collisions (Kolehmainen et al., 2017). In terms of experimental validation, to the best of our knowledge, currently there are no available experimental data on the role of the Young modulus on tribolectric charging during pneumatic conveying.

The pdfs of the electric charge per exiting particle, Q_{el}, are plotted in Fig. 7(b). Therein we can see that for Case 5, i.e. the case with the smallest

Case	$\mathrm{N_{in}}$	$\mathrm{N_{out}}$	$\frac{\rho(1-\nu_{\mathrm{p}}^2)}{E_{\mathrm{p}}}$ $\left[\frac{\mathrm{s}^2}{\mathrm{m}^2}\right]$	$\Delta Q_{\mathrm{pw}}^{\mathrm{av}}$ [pC]	$\lvert Q^{\mathrm{av}}\rvert$ [pC]	$\lvert Q_{\mathrm{n}}^{\mathrm{t}}\rvert$ $\left[\frac{\mu\mathrm{C}}{\mathrm{m}^2}\right]$
1	684168	508450	0.31	0.0243	0.0204	0.0723
6	621175	458310	0.42	0.0308	0.0270	0.0955
5	828502	621941	0.57	0.0416	0.0317	0.1122

Table 4: Effect of the material properties on powder electrification. N_{in} and N_{out} are the numbers of injected and exiting particles during the simulation. $\Delta Q_{\mathrm{pw}}^{\mathrm{av}}$ is the average charge transfer per wall-particle collision, Q^{av} is the (average) charge per exiting particle, and $Q_{\mathrm{n}}^{\mathrm{t}}$ is the total charge of the exiting particles normalized by the powder's surface area.

E_p, the probability to find particles with small charge is higher than for the other cases but it is less likely to find particles with intermediate charge (between -0.01 and -0.02 pC). This may be attributed to the aforementioned fact that smaller values of E_p lead to larger charge exchanges during particle-particle collisions and, therefore, to a more uniform distribution of the electric charge over the particles. It is worth clarifying that the above behavior is mainly attributed to E_p and not to the Poisson ratio ν_p, because the Poisson ratio varies only slightly in the cases examined herein.

Our numerical simulations further predicted that the main contribution of the material density to powder electrification is via the gravitational acceleration on the particles. Heavier particles tend to collide more often with the bottom part of the wall and, therefore, experience more wall-particle collisions. However, this is a secondary effect compared to the impact of the Young modulus. For example, in Case 5 the particles undergo fewer collisions with the wall. For example, the material of Case 5 is lighter and, consequently the particles undergo fewer collisions with the wall than in the other cases. Nonetheless, in Case 5 and due to the larger contact area, the charge exchanges with the wall are larger which leads to higher levels of powder electrification.

4.3. Effect of the powder mass-loading

In the context of our study, we performed simulations with different powder mass-loadings $\dot{m}$ by modifying the number of injected particles while keeping the particle diameter constant. More specifically, the mass loading in Case 7 was 50 % smaller than the one in the reference case, whereas in Case 8 it was ten times higher.

According to our numerical predictions, which are summarized in Table 5, the particle electrification is largely independent of the powder mass-loading.

Case	$\mathrm{N_{in}}$	$\mathrm{N_{out}}$	$\dot{m}$ $[\frac{\mathrm{g}}{\mathrm{s}}]$	$\Delta Q_\mathrm{pw}^\mathrm{av}$ [pC]	$\lvert Q^\mathrm{av}\rvert$ [pC]	$\lvert Q_\mathrm{n}^\mathrm{t}\rvert$ $[\frac{\mu\mathrm{C}}{\mathrm{m}^2}]$
7	342093	253769	5	0.0242	0.0203	0.0720
1	684168	508450	10	0.0243	0.0204	0.0723
8	3418426	2375525	50	0.0249	0.0208	0.0734

Table 5: Effect of the powder mass loading on powder electrification. N_in and N_out are the numbers of injected and exiting particles during the simulation. $\Delta Q_\mathrm{pw}^\mathrm{av}$ is the average charge transfer per wall-particle collision, Q^av is the average charge per exiting particle, and Q_n^t is the total charge of the exiting particles normalized by the powder's surface area.

In particular, both the wall-particle charge exchange and the average charge per particle remain constant. Similarly, the variations of the total charge normalized by the surface area of the powder are so small that can be attributed to numerical round-off errors. The same conclusion is drawn upon inspection of the pdf of the charge exchange during wall-particle collisions, as shown in Fig. 8(a). In particular, we verify that this pdf is completely insensitive to the powder mass-loading.

The pdf of the electric charge per exiting particle, Q_{el}, is plotted in Fig. 8(a). Therein we can identify some differences in the region of lightly charged particles. More specifically, the percentage of particles that are lightly charged increases with the mass loading. This is attributed to the fact that as the mass loadings increases, so does the number density of the particles. This means that at higher mass loadings there are relatively more particle-particle collisions which leads to a higher number of particles with small charges. Nonetheless, this does not bear any consequence to the global properties of the charge electrification. More specifically, the electrification of the entire powder is proportional to the mass loading, i.e. to the number of injected particles.

4.4. Effect of the inlet velocity

In this section we discuss our numerical simulations with different inlet velocities $\boldsymbol{u}_{\mathrm{in}}$. As mentioned in the Introduction, the increase of triboelectric charging with the transport (inlet) velocity is well established via both numerical studies and experiments. Our study focuses on the effect of the inlet

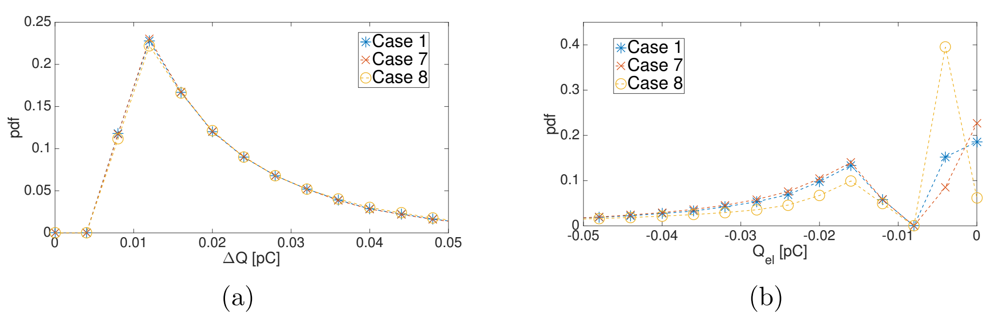

Figure 8: Effect of the powder mass loading on powder electrification. (a) Probability density function (pdf) of the charge exchange ΔQ during wall-particle collisions. (b) Probability density function (pdf) of the electric charge Q_{el} per exiting particle.

velocity on the wall-particle collisions and the average charge per particle at the pipe exit. To this end, we have considered Cases 9, 10, 1 and 11, which correspond to $\boldsymbol{u}_{\text{in}} = 10$, 20, 30 and 40 m/s, respectively. On the basis of these inlet velocities, the corresponding Reynolds numbers are $Re = 27000$, 54000, 82000, and 109000.

We first remark that due to aerodynamic drag, the mixture tends to mechanical equilibrium. In other words, the particle velocity $\boldsymbol{u}_{\text{p}}$ and the air velocity $\boldsymbol{u}_{\text{in}}$ tend to equilibrate. Therefore, when $\boldsymbol{u}_{\text{in}}$ increases, we expect $\boldsymbol{u}_{\text{p}}$ to increase by the same amount. Moreover, the parameter α_{pw} that is defined in Eq. (19) scales quadratically with $|\boldsymbol{u}_{\text{p}}|$. Moreover, the contact time Δt_{pw} of a wall-particle collision is inversely proportional to $|\boldsymbol{u}_{\text{p}}|$; see Eq.(20). We therefore expect that the charge transfer during a wall-particle collision to increase strongly at higher inlet velocities, which in turn would increase the powder electrification.

On the other hand, when $\boldsymbol{u}_{\text{p}}$ increases, the particles tend to spend less time in the pipe, which may lead to fewer wall-particle collisions. This in turn, contributes to the decrease of the powder electrification. In other words, changes of $\boldsymbol{u}_{\text{in}}$ may contribute to two different ways with regard to the charge accumulation in the powder.

The results provided in Table 6 show that even though the number of injected particles stays practically constant, the number of outgoing particles increases considerably with the inlet velocity. This is a direct consequence of the fact that at higher velocities, the particles exit the pipe faster. Our simulations further predicted the charge transfer per wall-particle collision, $\Delta Q_{\text{pw}}^{\text{av}}$, increases monotonically with the inlet velocity (equivalently, the Reynolds number Re).

We also observe that at the low range of Reynolds numbers, the average charge per particle $|Q^{\text{av}}|$ slightly drops when Re increases. This occurs because at the lowest Re, particles begin to settle down as they approach the end of the pipe. Consequently, they end up colliding more often with the wall. In fact, according to our simulations, the number of collisions in Case 9 is twice as much as in Case 10. This results to higher average charge per particle and higher total charge as Re decreases.

However, at the range of high Reynolds numbers, the opposite is true: the average charge exchange with the wall increases considerably and so does $|Q^{\text{av}}|$. We further remark that the total charge normalized by the surface area of powder exhibits exactly the same trends as $|Q^{\text{av}}|$ does. It is also interesting to note that for Case 9, the average charge per exiting particle $|Q^{\text{av}}|$ is higher

Case	$\mathrm{N_{in}}$	$\mathrm{N_{out}}$	Re	$\Delta Q_{\mathrm{pw}}^{\mathrm{av}}$ [pC]	$\lvert Q^{\mathrm{av}}\rvert$ [pC]	$\lvert Q_{\mathrm{n}}^{\mathrm{t}}\rvert$ $[\frac{\mathrm{\mu C}}{\mathrm{m^2}}]$
9	683192	403730	27000	0.0098	0.0188	0.0664
10	685192	495907	54000	0.0186	0.0161	0.0569
1	684168	508450	82000	0.0243	0.0204	0.0723
11	683946	511195	109000	0.0290	0.0244	0.0863

Table 6: Effect of the inlet velocity on powder electrification. N_{in} and N_{out} are the numbers of injected and exiting particles during the simulation. Re is the Reynolds number based on the inlet velocity, $\Delta Q_{\mathrm{pw}}^{\mathrm{av}}$ is the average charge transfer per wall-particle collision, Q^{av} is the average charge per exiting particle, and $Q_{\mathrm{n}}^{\mathrm{t}}$ is the total charge of the exiting particles normalized by the powder's surface area.

than the charge exchange per wall-particle collision $\Delta Q_{\mathrm{pw}}^{\mathrm{av}}$, just as in Cases 3 and 4. As mentioned above, this results from the large number of collisions with the wall.

For the cases with different inlet velocities considered herein, the distributions of the charge exchange with the wall ΔQ and the particle charge Q_{el} are plotted in Fig. 9. These plots confirm that as $\boldsymbol{u}_{\mathrm{in}}$ increases, the peak of the pdf occurs at higher charges. This is a direct consequence of the fact that the charge exchange during a wall-particle collision increases with the inlet velocity. Further, the pdfs become more disperse as $\boldsymbol{u}_{\mathrm{in}}$ increases. This is due to the fact that the number of particle-particle collisions increases monotonically with $\boldsymbol{u}_{\mathrm{in}}$. Similarly, the peak of the pdf for the particle charge shifts to higher charges. In other words, the percentage of particles that end up carrying a significant amount of charge also increases with $\boldsymbol{u}_{\mathrm{in}}$. In summary, we conclude that the electrification of a powder is quite sensitive to the inlet velocity and increases monotonically with it.

5. Conclusions

In this paper, we reported on our parametric studies of the effects of the particle properties and flow rates to the powder electrification during pneumatic transport. These were conducted via Large Eddy Simulation of the turbulent particle-laden flow that is developed inside a steel-made pipe. Our simulations predicted that, under constant mass loading, higher particle diameters increase considerably both the charge transfer during wall-particle collisions and the average charge per particle. Moreover, they lead to a more uniform distribution of charge among the particles because of the significant charge exchange that takes place during particle-particle collisions.

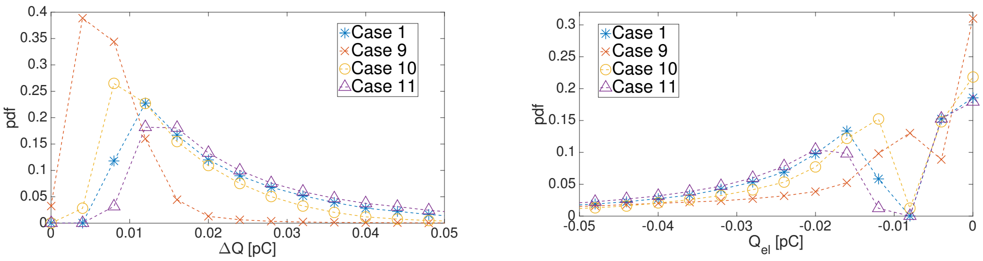

(a) (b)

Figure 9: Effect of the inlet velocity on powder electrification. (a) Probability density function (pdf) of the charge exchange ΔQ during wall-particle collisions. (b) Probability density function (pdf) of the electric charge Q_{el} per exiting particle.

As regards the material of the powder, it was shown that lower Young modulus favors significantly powder electrification because it leads to large contact areas during wall-particle collisions. Also, heavier particles collide more often with the bottom walls, due to gravity, which also enhances triboelectric charging. Finally, our simulations predicted higher inlet velocities increase significantly the charge transfer during wall-particle collisions. The average charge per particle, though, does not necessarily follow the same trend because at higher inlet velocities the particles exit the pipe faster and, therefore, collide with the wall less often. Further, we observed that the average charge per particle is quite insensitive to the powder mass loading. Finally, our simulations confirmed that the charge transfer during a wall-particle collision increases montonically with the inlet velocity. At high Reynolds numbers, this leads to higher charge per particle. However, at sufficiently low Re, reducing the inlet velocity can lead to an increase of the average particle charge due to the tendency of the particles to settle at the bottom wall. The results of our study can be used as guidelines for reducing triboelectric charging. The effect of certain parameters that are also expected to play a significant role, such as the contact potential of the wall-particle materials and the ambient humidity, has not been examined herein; this is a task that we intend to undertake in the future.

References

Bailey, A. G., 2001. The charging of insulator surfaces. J. Electrostat. 51–52, 81–90.

Baytekin, H. T., Patashisnki, A. Z. Branicki, M., Baytekin, B., Soh, S., Grzybowski, B. A., 2011. The mosaic of surface charge in contact electrification. Science 33, 308–312.

Caporaloni, M., Tampieri, F., Trombetti, F., Vittori, O., 1975. Transfer of particles in nonisotropic air turbulence. J. Atmos. Sci. 32, 565–568.

Davies, D. K., 1969. Charge Generation on Dielectric Surfaces. Br. J. Appl. Phys. D 2, 1533–1537.

Fath, W., Blum, C., Glor, M., Walther, C. D., 2013. Electrostatic ignition hazards due to pneumatic transport of flammable powders through insulating or dissipative tubes and hoses – new experiments and calculations. J. Electrostat. 71 (3), 377–382.

Fotovat, F., Bi, X. T., Grace, J. R., 2017. Electrostatics in gas-solid fluidized beds: a review. Chem. Eng. Sci. 173, 303–334.

Germano, M., Piomelli, U., Moin, P., Cabot, W. H., 1991. A dynamic subgrid-scale eddy viscosity model. Phys. Fluids A 3 (7), 1760–1765.

Glor, M., 2001. Overview of the occurrence and incendivity of cone discharges with case studies from industrial practice. J. Loss Prev. Process Ind. 14, 123–128.

Glor, M., 2003. Ignition hazard due to static electricity in particulate processes. Powder Technol. 135–136, 223–233.

Greason, W., 2000. Investigation of a test methodology for triboelectrification. J. Electrost. 49, 245–256.

Grosshans, H., Papalexandris, M. V., 2016a. Evaluation of the parameters influencing electrostatic charging of powder in a pipe flow. J. Loss Prev. Process Ind. 43, 83–91.

Grosshans, H., Papalexandris, M. V., 2016b. Large Eddy simulation of triboelectric charging in pneumatic powder transport. Powder Technol. 301, 1008–1015.

Grosshans, H., Papalexandris, M. V., 2016c. A model for the non-uniform contact charging of particles. Powder Technol. 305, 518–527.

Grosshans, H., Papalexandris, M. V., 2017a. Direct numerical simulation of triboelectric charging in a particle-laden turbulent channel flow. J. Fluid Mech. 818, 465–491.

Grosshans, H., Papalexandris, M. V., 2017b. Numerical study of the influence of the powder and pipe properties on electrical charging during pneumatic conveying. Powder Technol. 315, 227 – 235.

Grosshans, H., Papalexandris, M. V., 2017c. On the accuracy of the numerical computation of the electrostatic forces between charged particles. Powder Technol. 322, 185–194.

Grosshans, H., Papalexandris, M. V., 2018. Exploring the mechanism of interparticle charge diffusion. EPJ AP - Applied Physics 820, # 11101.

Grosshans, H., Szász, R.-Z., Fuchs, L., 2014. Development of an efficient statistical volumes of fluid–lagrangian particle tracking coupling method. Int. J. Num. Meth. Fluids 74 (12), 898–918.

Grosshans, H., Szász, R.-Z., Papalexandris, M. V., 2017. Modeling the electrostatic charging of a helicopter during hovering in dusty atmosphere. Aerosp. Sci. Technol. 64, 31–38.

Grosshans, H., Szász, R.-Z., Papalexandris, M. V., 2018. Influence of the rotor configuration on the electrostatic charging of helicopters. AIAA J. 56, 368–375.

Grötzbach, G., 1987. Direct numerical and Large Eddy simulation of turbulent channel flows. In: Chereminisoff, N. P. (Ed.), Encyclopedia of Fluid Mechanics. Vol. 6. Gulf, West Orange, NJ, pp. 1337–1391.

Gullbrand, J., Bai, X. S., Fuchs, L., 2001. High-order Cartesian grid method for calculation of incompressible turbulent flows. Int. J. Num. Meth. Fluids 36, 687–709.

Harper, W. R., 1951. The Volta effect as a cause of static electrification. Proc. Royal Soc. London Series A 205, 83–103.

Hockney, R., Eastwood, J., 1989. Computer Simulation Using Particles. Taylor and Francis.

Jang, G. S., Shu, C. W., 1996. Efficient implementation of weighted ENO schemes. J. Comput. Phys. 126, 202–228.

John, W., Reischl, G., Devor, W., 1980. Charge transfer to metal surfaces from bouncing aerosol particles. J. Aerosol Sci. 11 (2), 115–138.

Klinzing, G. E., 2018. A review of pneumatic conveying status, advances and projections. Powder Technol. 333, 78–90.

Kolehmainen, J., Ozel, A., Boyce, C. M., Sundaresan, S., 2017. Triboelectric charging of monodisperse particles in fluidized beds. AIChE J. 63, 1872–1891.

Kolehmainen, J., Ozel, A., Gu, Y., Shinbrot, T., Sundaresan, S., 2018. Effects of polarization on particle-laden flows. Phys. Rev. Lett. 124503, 1–5.

Kolniak, P. Z., Kuczynski, R., 1989. Numerical modeling of powder electrification in pneumatic transport. J. Electrostat. 23, 421–430.

Lackmann, J., 2007. B Mechanik. In: Grote, K., Feldhusen, J. (Eds.), Dubbel - Taschenbuch für den Maschinenbau. Springer.

Lacks, D. J., Duff, N., 2008. Nonequilibrium accumulation of surface species and triboelectric charging in single component particulate systems. Phys. Rev. Lett. 100, 188305.

LaMarche, K. R., Liu, X., Shah, S. K., Shinbrot, T., Glasser, B. J., 2009. Electrostatic charging during the flow of grains from a cylinder. Powder Technol. 195 (2), 158–165.

Lee, L. H., 1994. Dual mechanism for metal polymer contact electrification. J. Electrostat. 32, 1–29.

Lilly, D. K., 1992. A proposed modification of the germano subgrid-scale closure method. Phys. Fluids A 4 (3), 633–635.

Lowell, J., Rose-Innes, A. C., 1980. Contact electrification. Adv. Phys. 29, 947–1023.

Masui, N., Murata, Y., 1983. Electrification of polymer particles by impact on a metal plate. Jpn. J. Appl. Phys. 22, 1057–1062.

Matsusaka, S., Ando, K., Tanaka, Y., 2008. Development of electrostatic charge controller for particles in gases using centrifugal contact. J. Soc. Powder Technol. Jpn. 45, 380–386.

Matsusaka, S., Maruyama, H., Matsuyama, T., Ghadiri, M., 2010. Triboelectric charging of powders: a review. Chem. Eng. Sci. 64, 5781–5807.

Matsusaka, S., Oki, M., Masuda, H., 2007. Control of electrostatic charge on particles by impact charging. Adv. Powder Technol. 18, 229–244.

Matsuyama, T., Ogu, M., Yamamoto, H., Marijnissen, J., Scarlett, B., 2003. Impact charging experiments with single particles of hundred micrometre size. Powder Technol. 135–136, 14–22.

Matsuyama, T., Yamamoto, H., 1995. Electrification of single polymer particles by successive impacts with metal targets. IEEE Trans. Ind. Appl. 31, 1441–1445.

Mehrani, P., Bi, H. T., Grace, J. R., 2007. Bench-scale tests to determine mechanisms of charge generation due to particle-particle and particle-wall contact in binary systems of fine and coarse particles. Powder Technol. 173 (2), 73–81.

Murata, Y., Kittaka, S., 1979. Evidence of electron transfer as the mechanism of static charge generation by contact of polymers with metals. Jpn. J. Appl. Phys. 18, 421.

Nifuku, M., Katoh, H., 2003. A study on the static electrification of powders during pneumatic transportation and the ignition of dust cloud. Powder Technol. 135–136, 234–242.

Reeks, M. W., 1983. The transport of discrete particles in inhomogeneous turbulence. J. Aerosol Sci. 14, 729–739.

Saleh, K., Ndama, A. T., Guigon, P., 2011. Relevant parameters involved in tribocharging of powders during dilute phase pneumatic transport. Chem. Eng. Res. Des. 89 (12), 2582–2597.

Schiller, L., Naumann, A., 1935. A drag coefficient correlation. Z. Ver. Dtsch. Ing. 77, 318–320.

Schwindt, N., von Pidoll, U., Markus, D., Klausmeyer, U., Papalexandris, M., Grosshans, H., 2017. Measurement of electrostatic charging during pneumatic conveying of powders. J. Loss Prev. Process Ind. 49, 461–471.

Shinbrot, T., 2014. Granular electrostatics: Progress and outstanding questions. EPJ Special Topics 223 (11), 2241–2252.

Sirignano, W. A., 1999. Fluid Dynamics and Transport of Droplets and Sprays. Cambridge University Press, Cambridge.

Smeltzer, E. E., Weaver, M. L., Klinzing, G. E., 1982. Individual electrostatic particle interaction in pneumatic transport. Powder Technol. 33, 31–42.

Soo, S. L., 1971. Dynamics of Charged Suspensions. In: Topics in Current Aerosol Research. Pergamon Press, pp. 71–73.

Tanoue, K., Ema, A., Masuda, H., 1999. Effect of material transfer and work hardening of metal surface on the current generated by impact of particle. J. Chem. Eng. Jpn. 32, 544–548.

Tsuji, Y., Morikawa, Y., Shiomi, H., 1984. LDV measurements of an air-solid two-phase flow in a vertical pipe. J. Fluid Mech. 139, 417–434.

Wang, F. J., Zhu, J. X., Beekmans, J. M., 2000. Pressure gradient and particle adhesion in the pneumatic transport of cohesive fine powders. Int. J. Multiphase Flow 26, 245–265.

Watano, S., Saito, S., Suzuki, T., 2003. Numerical simulation of electrostatic charge in powder pneumatic conveying process. Powder Technol. 135–136, 112–117.

Wei, W., Gu, Z., 2015. Electrification of particulate entrained fluid flows - Mechanisms, applications, and numerical methodology. Phys. Rep. 600, 1–53.

Yamamoto, H., Scarlett, B., 1986. Triboelectric charging of polymer particles by impact. Part. Charact. 3, 117–121.

Yao, Y., Capecelatro, J., 2018. Competition between drag and coulomb interactions in turbulent particle-laden flows using a coupled-fluid–Ewald-summation based approach. Phys. Rev. Fluids 3, 034301.

Zhou, Z. Y., Kuang, S. B., Chu, K. W., Yu, A. B., 2010. Discrete particle simulation of particle-fluid flow: Model formulations and their applicability. J. Fluid Mech. 661, 482–510.

Zhu, H. P., Zhou, Z. Y., Yang, R. Y., Yu, A. B., 2008. Discrete particle simulation of particulate systems: A review of major applications and findings. Chem. Eng. Sci. 63, 5728–5770.

Zhu, K., Rao, S. M., Huang, Q. H., Wang, C.-H., Matsusaka, S., Masuda, H., 2004. On the electrostatics of pneumatic conveying of granular materials using electrical capacitance tomography. Chem. Eng. Sci. 59, 3201–3213.

Zhu, K., Rao, S. M., Wang, C. H., Sundaresan, S., 2003. Electrical capacitance tomography measurements on vertical and inclined pneumatic conveying of granular solids. Chem. Eng. Sci. 58, 4225–4245.